

High-Efficient Solar Cells Textured by Cu/Ag-Cocatalyzed Chemical Etching on Diamond Wire Sawing Multicrystalline Silicon

Wei Chen,^{†,‡} Yaoping Liu,^{*,†,‡,§} Juntao Wu,^{‡,§} Quansheng Chen,^{‡,§} Yan Zhao,^{‡,§} Yan Wang,^{†,‡} and Xiaolong Du^{*,†,‡,§}

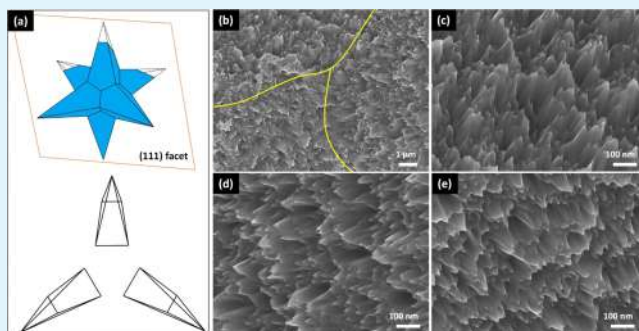
[†]Songshan Lake Materials Laboratory, Dongguan, Guangdong 523808, China

[‡]Key Laboratory for Renewable Energy, Institute of Physics, Chinese Academy of Sciences, Beijing 100190, China

[§]School of Physical Sciences, University of Chinese Academy of Sciences, Beijing 100049, China

ABSTRACT: We reported a novel texture method through one-step Cu/Ag-cocatalyzed chemical etching which can be widely used in the photovoltaic industry because of its simple and low-cost process. The etching mechanism of an inverted rectangular pyramid is the cooperation of Ag-catalyzed vertical etching and Cu-catalyzed lateral etching. In our texture method, neither saw damage removal nor post-treatment is needed. During the etching process, the digging holes by Ag-catalyzed etching and enlarging holes by Cu-catalyzed etching completed at the same step. Benefiting from the excellent light-trapping and passivation effect of the inverted rectangular pyramid, diamond wire sawing multicrystalline silicon (mc-Si) Al-BSF solar cells with a super high efficiency of 19.49% had been obtained.

KEYWORDS: metal-catalyzed chemical etching, Cu/Ag-cocatalyzed chemical etching, inverted rectangular pyramid, diamond wire sawing, silicon solar cells



INTRODUCTION

High efficiency and low cost are always the main drives of the photovoltaic (PV) industry. Up to now, multicrystalline silicon (mc-Si) solar cells still account for the most share of the PV market.¹ Slurry wire sawing (SWS) has been used to slice silicon ingots into thin wafers for decades. In order to further reduce the cost, diamond wire sawing (DWS) is developing rapidly. Compared with SWS, DWS has the advantages of higher slicing speed and less thickness of the saw damage layer,^{2–4} which greatly reduces the manufacturing cost. Thus, DWS is becoming the mainstream slicing technique to cut the silicon ingots into wafers in the short run. Unfortunately, due to the different surface structure of the DWS Si wafer from the SWS one, the conventional HF/HNO₃ acidic solution texture does not work well for DWS ones. The reason is that the amorphous Si layer caused by DWS would hinder the etching process which was confirmed by Raman spectroscopy, resulting in relatively high surface reflectivity.⁵ Meanwhile, the visible saw marks remaining on the DWS Si surface will also decrease solar cell's efficiency.⁶

Thus, for the texturization of DWS mc-Si, an effective texture method is desperately required. In recent years, black silicon (B-Si) has drawn a lot of attention because of its superior light-trapping effect. B-Si can be fabricated by reactive ion etching,^{7,8} laser-based approach,⁹ microwave and ICP-CCP plasma texturing,¹⁰ atmospheric pressure F₂-based dry etching,^{11,12} and plasma immersion ion implantation.^{13,14}

Among them, metal-assisted chemical etching (MACE) is the most cost-effective method to prepare B-Si during mass production. What is more, the MACE method will work for virtually any surface roughness, even though the DWS wafer.¹⁵ Normally, the saw damage layer must be removed before MACE and nanowire or nanopore silicon structures with a high aspect ratio are formed by the mostly used Ag-assisted chemical etching. However, such highly nanostructured B-Si will introduce more electron–hole recombination and surface recombination. In order to balance the optical and the electrical losses, a post treatment process must be used by either acid¹⁵ or alkali solutions,³ which causes additional procedure and cost. More recently, Cu-assisted chemical etching (CACE) had been reported to fabricate the inverted pyramid in the micrometer scale, which had simultaneous realization of excellent optical and electrical properties.^{16–18} However, the inverted pyramid texturization technique cannot be applied directly on mc-Si wafers because the randomly oriented grains in mc-Si wafers can cause color differences after the anisotropic etching of CACE.

In this work, as inspired by the vertical and lateral etching behavior resulted from Ag and Cu catalysis, respectively, a novel, cost-effective, and one-step Cu/Ag-cocatalyzed chemical

Received: January 13, 2019

Accepted: February 19, 2019

etching method without pre or post-treatment is developed. Three etched structures based on single crystal silicon (c-Si) (100), (110), and (111) oriented wafers were used to investigate the etching mechanism. The obtained inverted rectangular pyramidal structure has the characteristics of low reflectivity and easy passivation, along with little color differences, which is very suitable for mc-Si. Because of its superior light-trapping and structure characteristics, a super high efficiency of 19.49% based on AL-BSF mc-Si solar cells had been obtained. Besides, the longest processing time is 210 s, making it very facile to the current mass production.

RESULTS AND DISCUSSION

The nanostructure with a high aspect ratio is shown in Figure 1a, which was obtained through Ag-catalyzed chemical etching

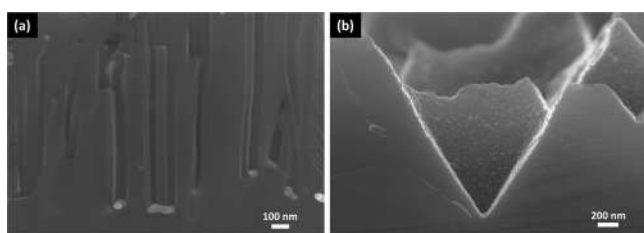


Figure 1. Scanning electron microscopy (SEM) images of the cross-sectional view: (a) B-Si by Ag-catalyzed chemical etching, (b) inverted pyramid by Cu-catalyzed chemical etching.

on the polished Si(100) wafer. The mechanism of Ag-catalyzed chemical etching had been systematically studied previously.^{19–24} Silicon beneath the Ag nanoparticles will be etched first, forming shallow-pit structures, accompanied by the sinking of Ag nanoparticles into the structures. With the prolongation of etching time, the nanowire arrays finally formed because of the continuous sinking of the Ag nanoparticles. As can be seen in Figure 1a, Ag clusters are found to lie at the bottom of nanowire arrays. Despite its low reflectivity, this highly nanostructured B-Si cannot be used for the fabrication of solar cells without post treatment.²⁵ Figure 1b shows the cross-sectional inverted pyramid fabricated by Cu-catalyzed chemical etching.^{16,26} The formation mechanism of the inverted pyramid lies in the anisotropic deposition of Cu nanoparticles on the Si surface, leading to the anisotropic etching of Si.^{16,17,27} Except for the excellent light-trapping effect, the inverted pyramid structure also has good passivation effect, which benefits the SiN_x deposition and metal-electrode filling.^{28,29} However, the inverted pyramid will cause color differences among different grains in the mc-Si wafer. As discussed above, the question of whether there is a facile method to fabricate structures with low reflectivity and easy surface passivation whereas leading to a minimum reflection distribution between grains of mc-Si still needs to be answered. Thus, by taking advantage of Ag-catalyzed vertical etching and Cu-catalyzed lateral etching, a novel inverted rectangular pyramid texture with excellent light-trapping ability and passivation effect is obtained.

To clarify the Cu/Ag-cocatalyzed etching mechanism, three textured structures based on Si(100), (110), and (111) wafers were investigated by using this method. Figure 2a,b displays the SEM images of the p-Si (100) substrate after being etched in the Cu/Ag-cocatalyzed solution for 210 s followed by removing of metal nanoparticles by concentrated nitric acid.

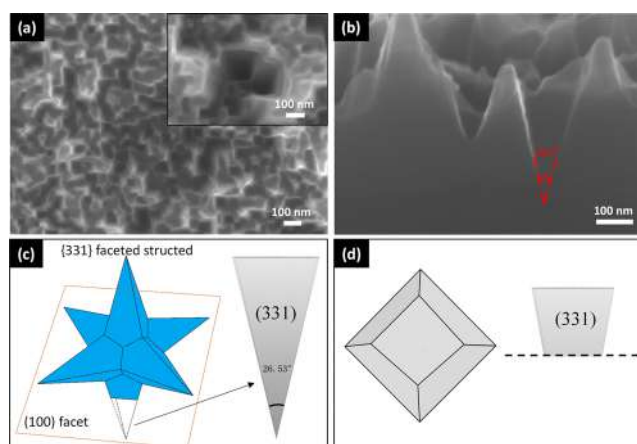


Figure 2. Morphology of the Cu/Ag-cocatalyzed chemical etching structure on Si(100) wafers: (a) top view, (b) cross-sectional view. Simulated schematics of {331}-faceted tetrahexahedron and {331}-faceted inverted rectangular pyramids (c), and truncated inverted rectangular pyramid (d).

Quadrilateral-shaped structures with diameter ranging from 50 to 350 nm are found in Figure 2a and some of them are overlapping to each other. As can be seen in Figure 2b, funnel-shaped structures with depth ranging from 120 to 500 nm were obtained. The etched structure is much different from that obtained by using single Ag or CACE. The measured apex angle of the funnel-shaped structure is 26.5°, which is consistent with the apex angle (26.53°) of the inverted rectangular pyramid bounded by {331} planes. The structure formed by {331} facets is a tetrahexahedron with six rectangular pyramids along the axis of the coordinate. The inverted rectangular pyramid was obtained by using the (100) plane to incise the {331}-faceted structure, as shown in Figure 2c. The aspect ratio of the {331}-faceted inverted rectangular pyramid is three times that of the standard inverted pyramid composed by {111} facets, as a result, some of the inverted rectangular pyramids become the inverted quadrangular frustum pyramid, as the simulated schematics shown in Figure 2d. Both the top and cross-sectional inverted rectangular pyramid shown in Figure 2a,b are basically the same as the simulation results. The reflectance of the structure varied with the depth of the inverted quadrangular frustum pyramid, generally decreased with the increased depth, reached the minimum when the structure became a fully inverted rectangular pyramid.

The above discussion shows that the formation mechanism of the inverted rectangular pyramid is Cu and Ag-cocatalyzed in the HF/H₂O₂ solutions. We have formerly fabricated the inverted pyramid structure in the micrometer size by Cu-assisted anisotropic chemical etching of Si. Because of the lower redox potential of Cu²⁺/Cu, the etching of the Si surface is limited, either inverted pyramids or shallow pits with lower aspect ratio were demonstrated,^{16,17,27,30} which means that lateral etching is much easier for CACE. While, for Ag-catalyzed chemical etching, nanowire or nanopore silicon structures with a high aspect ratio will be fabricated. Because of the much higher redox potential of Ag⁺/Ag, Ag particles can be easily trapped vertically into the silicon during the etching process, as the schematics shown in Figure 3, indicating that vertical etching is much easier for Ag-assisted chemical etching.²² Thus, the etching mechanism of the inverted

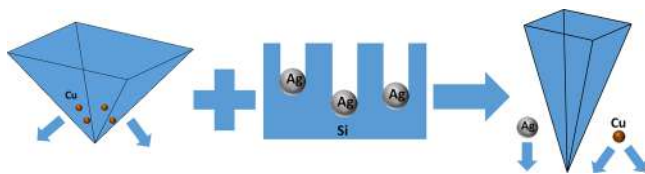
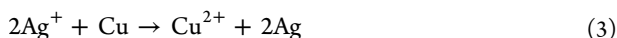


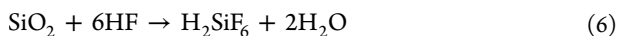
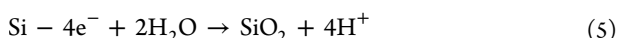
Figure 3. Schematics of the etching process by single Cu- and Ag-catalyzed chemical etching and Cu/Ag-cocatalyzed chemical etching.

rectangular pyramid is a cooperation of Cu-catalyzed lateral etching and Ag-catalyzed vertical etching. That is to say, in our texture method, digging holes by Ag-catalyzed etching and enlarging holes by Cu-catalyzed etching completed at the same step. It is worth mentioning that no Cu nanoparticles were found on the Si surface, which was confirmed by energy-dispersive spectroscopy. The reason is that, due to the replacement reaction, the Cu nanoparticles can obtain holes from Ag^+ ions and become Cu^{2+} ions. At the same time, Ag^+ ions were reduced to Ag nanoparticles. Besides, Cu nanoparticles can also be oxidized by the hydrogen peroxide, while it is more difficult for hydrogen peroxide to oxidize Ag nanoparticles. The possible reactions are as follows:

For the Cu/Ag redox process



For the silicon dissolution process



It is important to note that the reaction mechanism in this paper is much different from that reported by Wang and Chen³¹ and Zheng et al.,³² in which low concentration of Ag^+ is used to accelerate the etching rate of Cu. Besides, before the MACE process, the saw damage layer must be removed by acid texture, and the final etched structures are still nanopores which need a post-treatment to enlarge the diameter of the nanopores.

Figure 4 shows the simulated schematics of $\{331\}$ -faceted tetrahexahedron and two orientations of $\{331\}$ -faceted

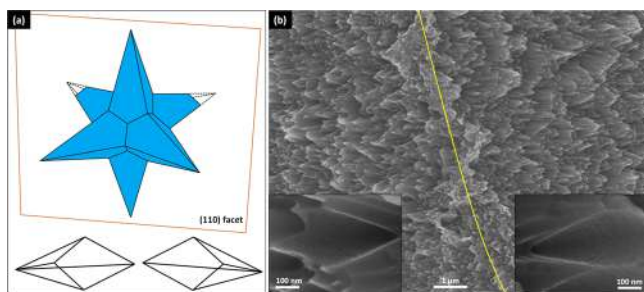


Figure 4. (a) Simulated schematics of $\{331\}$ -faceted tetrahexahedron and two orientations of $\{331\}$ -faceted inverted rectangular pyramids on (110)-oriented wafers, (b) corresponding SEM images of (a). The highlighted yellow line in (b) represents the boundary between the two inverted rectangular pyramids.

inverted rectangular pyramids on Si(110) wafers as well as the corresponding structures etched by Cu/Ag-cocatalyzed solutions for 210 s on Si(110) wafers. The simulation method is using the (110) crystal face to intersect with the $\{331\}$ -faceted tetrahexahedron and intersect with two of the rectangular pyramids. The top view of the intersect structure on the (110) surface is rhombus-shaped inverted rectangular pyramids, as shown in Figure 4a. Figure 4b shows the SEM images of the corresponding structures etched on (110) oriented wafers and the insets show the amplification SEM images, which are consistent with the simulation ones. We formerly fabricated a rhombus-like structure on Si(110) wafers by CACE,²⁶ which is much different from the structure obtained by Cu/Ag-cocatalyzed chemical etching. However, for Cu/Ag-cocatalyzed chemical etching, there are two orientation inverted rectangular pyramids on the (110) surface because of two of the rectangular pyramids are intersected by the (110) plane.

As for the (111)-oriented wafers, we obtained three orientation inverted rectangular pyramid-like structures using the same simulation method because three of the rectangular pyramids are intersected by the (111) plane. The simulated schematics on the (111) surface are shown in Figure 5a and the SEM images of the corresponding etched structures are listed in Figure 5b–e. These results reconfirm the correctness of our simulations. The structure etched by Cu/Ag-cocatalyzed chemical etching is also much different from the hexagonal and triangular structures etched by single CACE,²⁶ and their average reflectance differences will be discussed in the following. However, only nanostructures (nanowire or nanopore) are obtained for single Ag-assisted chemical etching, regardless of the silicon orientation.^{21,24,33,34}

For raw DWS mc-Si, although it consists of crystallites with different orientations, the texture is also effective by Cu/Ag-cocatalyzed etching. As shown in Figure 6a, damages are irregularly distributed on the as-cut DWS mc-wafers, such as damaged pits, cracks, and smooth parallel marks,³ while most of the visible saw marks are removed after being etched in 4.6 M HF, 0.44 M H_2O_2 , 4 mM AgNO_3 , and 20 mM $\text{Cu}(\text{NO}_3)_2$ mixture for 210 s at room temperature. The inverted rectangular pyramid Si surface fabricated by Cu/Ag-cocatalyzed etching is very uniform even among the different crystal orientations, as seen in Figure 6b. The etched structure on DWS mc-Si is also the inverted rectangular pyramid lined by $\{331\}$ planes, as shown in Figure 6c, the measured apex angle is 26.5° which is consistent with the apex angle (26.53°) bounded by $\{331\}$ planes. Figure 6d shows the simulated inverted rectangular pyramid on the (112) plane. The simulation method is using the (112) crystal face to intersect with the $\{331\}$ -faceted tetrahexahedron. The morphology of the etched structure is almost the same as the simulated one which further verifies the mechanism of Cu/Ag-cocatalyzed chemical etching. The reflectivity of the inverted rectangular pyramid on different oriented Si wafers has been measured. The average reflectivity (\bar{R}) is calculated as follows

$$\bar{R} = \frac{\int_{300 \text{ nm}}^{1000 \text{ nm}} R(\lambda) \cdot S(\lambda) d\lambda}{\int_{300 \text{ nm}}^{1000 \text{ nm}} S(\lambda) d\lambda} \quad (7)$$

where $S(\lambda)$ is the solar flux under AM1.5 standard conditions and $R(\lambda)$ is the measured reflectance. As shown in Figure 7, the \bar{R} from 300 to 1000 nm is 8.34, 11.38, and 13.01% for

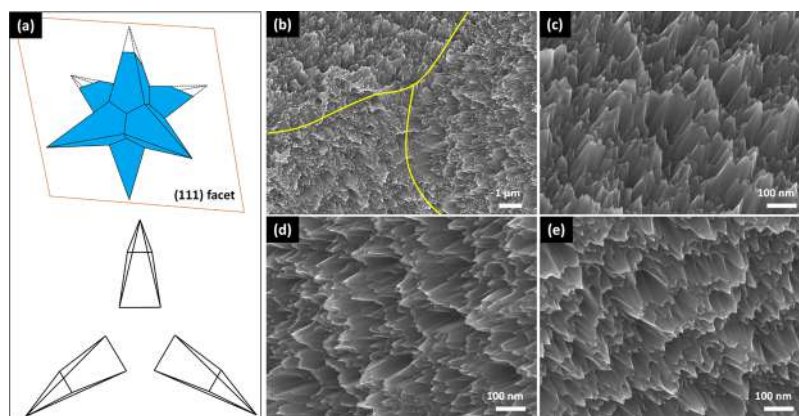


Figure 5. (a) Simulated schematics of $\{331\}$ -faceted tetrahedron and three orientations of $\{331\}$ -faceted inverted rectangular pyramids on (111)-oriented wafers, (b–e) corresponding SEM images of (a). The highlighted yellow line in (b) represents the boundary of the three inverted rectangular pyramids.

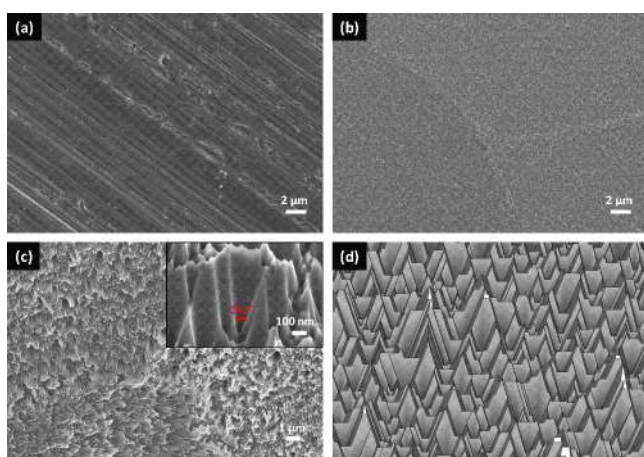


Figure 6. (a) As-cut morphologies for DWS mc-Si, (b) etched structure by Cu/Ag-cocatalyzed chemical etching, (c) magnified image of (b); (d) simulated $\{331\}$ -faceted inverted rectangular pyramid on (112)-oriented wafers.

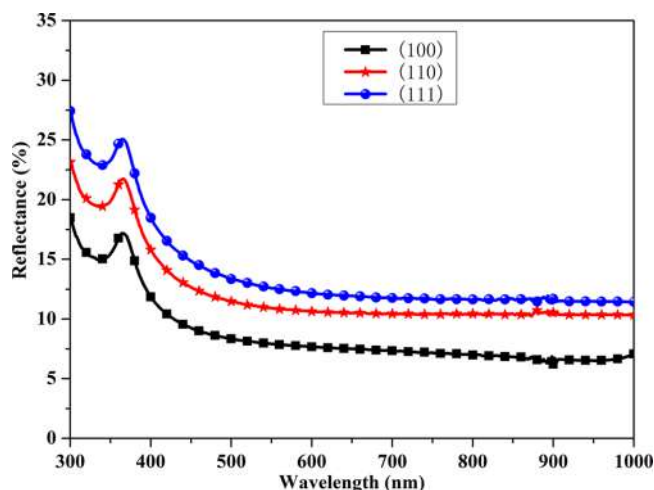


Figure 7. Reflectance spectra of Si(100), (110), and (111) substrates etched by Cu/Ag-cocatalyzed chemical etching.

(100), (110), and (111) surfaces, respectively, indicating that the maximum reflectivity differences of the DWS mc-Si are lower than 5%, while it is more than 20% for the standard

inverted pyramid,²⁶ and the reflectivity differences will further decrease to about 1% after the deposition of silicon nitride. What is more, the (100) crystal grains account for a very small proportion of the entire DWS mc-Si surface. Thus, the color differences on inverted rectangular pyramid DWS mc-Si are comparable to those of the acid-textured SWS mc-Si.

A standard Al-BSF solar cell process was applied on Cu/Ag-cocatalyzed etching of DWS mc-Si (labeled MCT-DWS). For comparison, solar cells based on the SWS and DWS mc-Si silicon wafers textured by conventional acidic solutions also have been fabricated on the same production line (labeled AT-SWS and AT-DWS). All the used wafers are from the same ingot and they are also randomized from different locations of ingot. For the detailed solar cell fabrication process, please refer to our previous work.²⁸

Figure 8 presents the reflectance and external quantum efficiency (EQE) spectra of the AT-SWS, AT-DWS, and MCT-

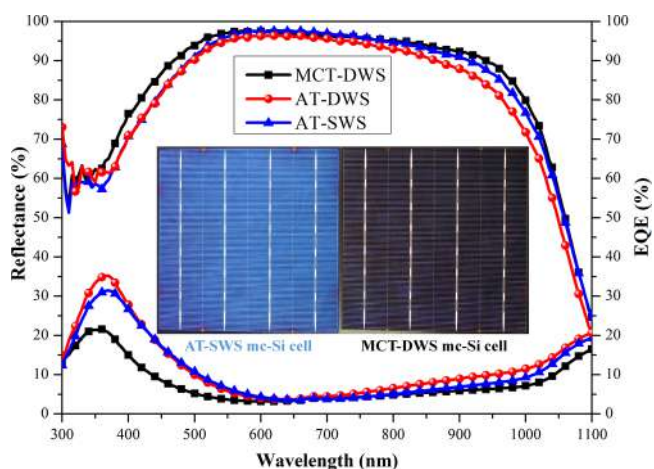


Figure 8. Reflectance and EQE spectra of the AT-SWS, AT-DWS, and MCT-DWS mc-Si solar cells from 300 to 1100 nm. The inset shows photographs of AT-SWS and MCT-DWS solar cells.

DWS mc-Si solar cells. The inset shows photographs of AT-SWS and MCT-DWS solar cells. The \bar{R} of the as-etched AT-SWS, AT-DWS, and MCT-DWS mc-Si is 25.15, 30.31, and 12.08%, respectively, and is reduced to 6.90% for AT-SWS, 8.76% for AT-DWS, and 3.25% for MCT-DWS, respectively, after SiN_x antireflection layer deposition. Because of the

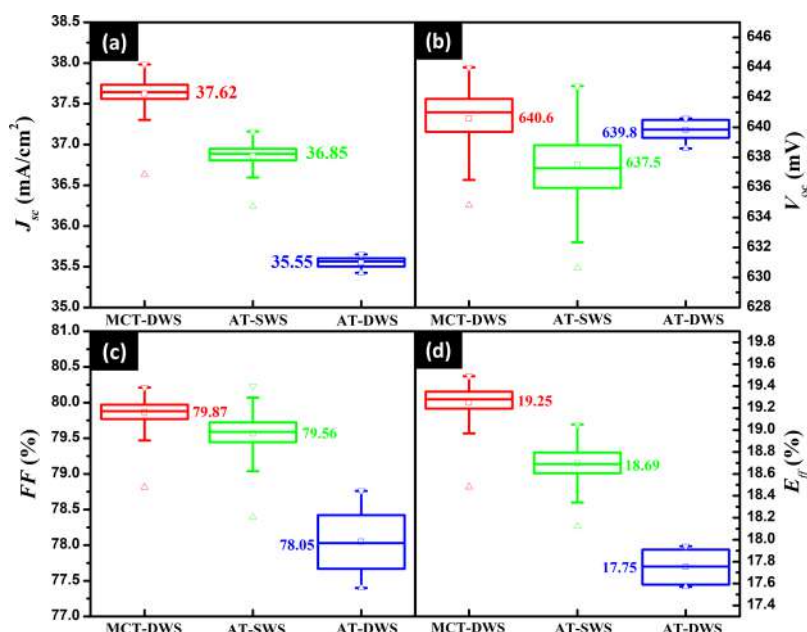


Figure 9. Box plot of cell performance: (a) J_{sc} , (b) V_{oc} , (c) FF, and (d) E_{ff} for AT-SWS, AT-DWS, and MCT-DWS mc-Si solar cells. The box plot shows the lower quartile, median, and upper quartile and the symbol \square , \triangle , and ∇ represent the mean, maximum, and minimum of the data, respectively.

structural characteristics of the inverted rectangular pyramid, the reflectivity between different grains is so small that the color differences in the MCT-DWS mc-Si solar cell are comparable to the AT-SWS mc-Si cell as the inset shown in Figure 8. The appearance of the MCT-DWS cells is dark blue, in contrast to the blue of AT-SWS cells. Because of the insufficient texturing by HF/HNO₃ solutions, the reflectivity of AT-DWS is still very high, even after the deposition of the SiN_x layer. While, as for MCT-DWS mc-Si, the \bar{R} is low enough over the whole range of wavelength due to the superior light-trapping effect of the inverted rectangular pyramid. The EQE of AT-SWS-, AT-DWS-, and MCT-DWS-based solar cells is tested to fully understand the influence of electrical and optical properties on the performance of solar cells. Obviously, the EQE of MCT-DWS is the highest in the whole wavelength range, which implies that both the lower reflectance and better passivation of the inverted rectangular pyramid attribute to the performance of the cells. However, the lower EQE value of AT-DWS-based solar cells in the long wavelength is attributed to the severe electric loss which was caused by the still visible saw marks after acid texture.

Figure 9a–d illustrates the box plot of the main electric performance parameters including short-circuit current density (J_{sc}), open-circuit voltage (V_{oc}), fill factor (FF), and conversion efficiency (E_{ff}) of the AT-DWS, AT-SWS, and MCT-DWS samples. The sample quantity of AT-DWS, AT-SWS, and MCT-DWS is 50, 400, and 1200 slices, respectively. The solar cell efficiency is tested under AM1.5 illumination with an area of 15.6×15.6 cm². Our best MCT-DWS solar cell efficiency is as high as 19.49%, which implies that the texturization of DWS mc-Si with the Cu/Ag-cocatalyzed chemical etching method is effective. What is more, the mean efficiency of the 1200 slices MCT-DWS cells has reached 19.25% with a J_{sc} of 37.62 mA/cm², V_{oc} of 640.6 mV, and FF of 79.87%, which is 0.56% absolute higher than the AT-SWS cells and 1.5% absolute higher than the AT-DWS cells. Because of the superior light-trapping and passivation effect of the inverted rectangular

pyramid together with the uniform surface, the J_{sc} of 37.62 mA/cm² is much higher than 36.85 mA/cm² of AT-SWS solar cells, together with a V_{oc} of 640.6 mV which is 3.1 mV higher than the production line. However, for AT-DWS solar cells, the much lower E_{ff} is resulting from the still visible saw marks and higher reflectance which not only deteriorates the electrical performance but also decreases light absorption. That is, the serious saw marks will give rise to the nonuniform p–n junction depth and poor finger contact to the silicon, which will greatly decrease FF.⁶

CONCLUSIONS

In summary, the inverted rectangular pyramid fabricated by the novel Cu/Ag-cocatalyzed chemical etching method simultaneously realized the excellent light-trapping and passivation effect. A highest efficiency of 19.49% based on DWS mc-Si had been obtained on an industrial production line. The etching mechanism of the inverted rectangular pyramid is the cooperation of Ag-catalyzed vertical etching and Cu-catalyzed lateral etching. The low cost, one-step texturing method without pre or post-treatment and maximum 210 s processing time, which not only solves the texturization problem of DWS mc-Si, but also opens up new prospects for the application of efficient solar cells.

EXPERIMENTAL METHODS

P-type single crystal silicon (c-Si) wafers with (100), (110), and (111) oriented and p-type commercially used 15.6×15.6 cm² DWS multicrystalline silicon wafers were used to investigate the texturing process. The inverted rectangular pyramid texture was obtained by the truly one-step Cu/Ag-cocatalyzed chemical etching, containing 4.6 M HF, 0.44 M H₂O₂, 4 mM AgNO₃, and 20 mM Cu(NO₃)₂, with about 3 μ m etching depth on each side. After texturization, concentrated HNO₃ was used to remove the metal nanoparticles on the Si surface, followed by a standard RCA cleaning. Then, the Al-BSF solar cells were fabricated on a current production line. Detailed processes and test methods have been introduced in our previous work.²⁸

AUTHOR INFORMATION

Corresponding Authors

*E-mail: ypliu@iphy.ac.cn (Y.L.).

*E-mail: xldu@iphy.ac.cn (X.D.).

ORCID

Yaoping Liu: 0000-0002-3881-1904

Notes

The authors declare no competing financial interest.

ACKNOWLEDGMENTS

This work was supported by the Science and Technology Department of Jiangsu Province (Technological Achievements Transformation Project, grant no. BA2017137) and National Science Foundation of China (grant nos. 11675280, 61874139, and 11674405). The authors are grateful for the technical support from the Laboratory of Microfabrication in Institute of Physics, Chinese Academy of Sciences.

REFERENCES

- (1) Mann, S. A.; de Wild-Scholten, M. J.; Ethenakis, V. M.; van Sark, W. G. J. H. M.; Sinke, W. C. The energy payback time of advanced crystalline silicon PV modules in 2020: a prospective study. *Prog. Photovoltaics Res. Appl.* **2014**, *22*, 1180–1194.
- (2) Yu, X.; Wang, P.; Li, X.; Yang, D. Thin Czochralski Silicon Solar Cells Based on Diamond Wire Sawing Technology. *Sol. Energy Mater. Sol. Cells* **2012**, *98*, 337–342.
- (3) Zhuang, Y. F.; Zhong, S. H.; Huang, Z. G.; Shen, W. Z. Versatile Strategies for Improving the Performance of Diamond Wire Sawn Mc-Si Solar Cells. *Sol. Energy Mater. Sol. Cells* **2016**, *153*, 18–24.
- (4) Zha, J.; Wang, T.; Pan, C.; Chen, K.; Hu, F.; Pi, X.; Su, X. Constructing Submicron Textures on Mc-Si Solar Cells via Copper-Catalyzed Chemical Etching. *Appl. Phys. Lett.* **2017**, *110*, 093901.
- (5) Kawasegi, N.; Morita, N.; Yamada, S.; Takano, N.; Oyama, T.; Ashida, K. Etch Stop of Silicon Surface Induced by Tribo-Nanolithography. *Nanotechnology* **2005**, *16*, 1411–1414.
- (6) Chen, K.; Liu, Y.; Wang, X.; Zhang, L.; Su, X. Novel Texturing Process for Diamond-Wire-Sawn Single-Crystalline Silicon Solar Cell. *Sol. Energy Mater. Sol. Cells* **2015**, *133*, 148–155.
- (7) Liu, S.; Niu, X.; Shan, W.; Lu, W.; Zheng, J.; Li, Y.; Duan, H.; Quan, W.; Han, W.; Wronski, C. R.; et al. Improvement of Conversion Efficiency of Multicrystalline Silicon Solar Cells by Incorporating Reactive Ion Etching Texturing. *Sol. Energy Mater. Sol. Cells* **2014**, *127*, 21–26.
- (8) Xiao, G.; Liu, B.; Liu, J.; Xu, Z. The Study of Defect Removal Etching of Black Silicon for Solar Cells. *Mater. Sci. Semicond. Process.* **2014**, *22*, 64–68.
- (9) Kontermann, S.; Gimpel, T.; Baumann, A. L.; Guenther, K.-M.; Schade, W. Laser Processed Black Silicon for Photovoltaic Applications. *Energy Procedia* **2012**, *27*, 390–395.
- (10) Cho, C.-W.; Lee, J.-H.; Riu, D.-H.; Kim, C.-Y. Fast Responsive Gas Sensor of Vertically Aligned Fluorine-Doped Tin Oxide Nanorod Thin Film. *Jpn. J. Appl. Phys.* **2012**, *51*, 045001.
- (11) Kafle, B.; Mannan, A.; Freund, T.; Clochard, L.; Duffy, E.; Hofmann, M.; Rentsch, J.; Preu, R. Nanotextured Multicrystalline Al-BSF Solar Cells Reaching 18% Conversion Efficiency Using Industrially Viable Solar Cell Processes. *Phys. Status Solidi RRL* **2015**, *9*, 448–452.
- (12) Kafle, B.; Schön, J.; Fleischmann, C.; Werner, S.; Wolf, A.; Clochard, L.; Duffy, E.; Hofmann, M.; Rentsch, J. On the Emitter Formation in Nanotextured Silicon Solar Cells to Achieve Improved Electrical Performances. *Sol. Energy Mater. Sol. Cells* **2016**, *152*, 94–102.
- (13) Xia, Y.; Liu, B.; Liu, J.; Shen, Z.; Li, C. A Novel Method to Produce Black Silicon for Solar Cells. *Sol. Energy* **2011**, *85*, 1574–1578.
- (14) Shen, Z.; Liu, B.; Xia, Y.; Liu, J.; Liu, J.; Zhong, S.; Li, C. Black Silicon on Emitter Diminishes the Lateral Electric Field and Enhances the Blue Response of a Solar Cell by Optimizing Depletion Region Uniformity. *Scr. Mater.* **2013**, *68*, 199–202.
- (15) Kumagai, A. Texturization Using Metal Catalyst Wet Chemical Etching for Multicrystalline Diamond Wire Sawn Wafer. *Sol. Energy Mater. Sol. Cells* **2015**, *133*, 216–222.
- (16) Wang, Y.; Yang, L.; Liu, Y.; Mei, Z.; Chen, W.; Li, J.; Liang, H.; Kuznetsov, A.; Xiaolong, D. Maskless Inverted Pyramid Texturization of Silicon. *Sci. Rep.* **2015**, *5*, 10843.
- (17) Wang, Y.; Liu, Y.; Yang, L.; Chen, W.; Du, X.; Kuznetsov, A. Micro-Structured Inverted Pyramid Texturization of Si Inspired by Self-Assembled Cu Nanoparticles. *Nanoscale* **2017**, *9*, 907–914.
- (18) Yang, L.; Liu, Y.; Chen, W.; Wang, Y.; Liang, H.; Mei, Z.; Kuznetsov, A.; Du, X. Interface Engineering of High Efficiency Organic-Silicon Heterojunction Solar Cells. *ACS Appl. Mater. Interfaces* **2016**, *8*, 26–30.
- (19) Hsu, C.-H.; Wu, J.-R.; Lu, Y.-T.; Flood, D. J.; Barron, A. R.; Chen, L.-C. Fabrication and Characteristics of Black Silicon for Solar Cell Applications: An Overview. *Mater. Sci. Semicond. Process.* **2014**, *25*, 2–17.
- (20) Li, S.; Ma, W.; Chen, X.; Xie, K.; Li, Y.; He, X.; Yang, X.; Lei, Y. Structure and Antireflection Properties of SiNWs Arrays Form Mc-Si Wafer through Ag-Catalyzed Chemical Etching. *Appl. Surf. Sci.* **2016**, *369*, 232–240.
- (21) Huang, Z.; Geyer, N.; Werner, P.; de Boer, J.; Gösele, U. Metal-Assisted Chemical Etching of Silicon: A Review. *Adv. Mater.* **2011**, *23*, 285–308.
- (22) Liu, Y.; Lai, T.; Li, H.; Wang, Y.; Mei, Z.; Liang, H.; Li, Z.; Zhang, F.; Wang, W.; Kuznetsov, A. Y.; et al. Nanostructure Formation and Passivation of Large-Area Black Silicon for Solar Cell Applications. *Small* **2012**, *8*, 1392–1397.
- (23) Peng, K.; Fang, H.; Hu, J.; Wu, Y.; Zhu, J.; Yan, Y.; Lee, S. Metal-Particle-Induced, Highly Localized Site-Specific Etching of Si and Formation of Single-Crystalline Si Nanowires in Aqueous Fluoride Solution. *Chem.—Eur. J.* **2006**, *12*, 7942–7947.
- (24) Fang, H.; Wu, Y.; Zhao, J.; Zhu, J. Silver Catalysis in the Fabrication of Silicon Nanowire Arrays. *Nanotechnology* **2006**, *17*, 3768–3774.
- (25) Ying, Z.; Liao, M.; Yang, X.; Han, C.; Li, J.; Li, J.; Li, Y.; Gao, P.; Ye, J. High-Performance Black Multicrystalline Silicon Solar Cells by a Highly Simplified Metal-Catalyzed Chemical Etching Method. *IEEE J. Photovoltaics* **2016**, *6*, 888–893.
- (26) Chen, W.; Liu, Y.; Yang, L.; Wu, J.; Chen, Q.; Zhao, Y.; Wang, Y.; Du, X. Difference in Anisotropic Etching Characteristics of Alkaline and Copper Based Acid Solutions for Single-Crystalline Si. *Sci. Rep.* **2018**, *8*, 3408.
- (27) Lu, Y.-T.; Barron, A. R. Anti-Reflection Layers Fabricated by a One-Step Copper-Assisted Chemical Etching with Inverted Pyramidal Structures Intermediate between Texturing and Nanopore-Type Black Silicon. *J. Mater. Chem. A* **2014**, *2*, 12043.
- (28) Yang, L.; Liu, Y.; Wang, Y.; Chen, W.; Chen, Q.; Wu, J.; Kuznetsov, A.; Du, X. 18.87%-Efficient Inverted Pyramid Structured Silicon Solar Cell by One-Step Cu-Assisted Texturization Technique. *Sol. Energy Mater. Sol. Cells* **2017**, *166*, 121–126.
- (29) Kafle, B.; Freund, T.; Werner, S.; Schon, J.; Lorenz, A.; Wolf, A.; Clochard, L.; Duffy, E.; Saint-Cast, P.; Hofmann, M.; et al. On the Nature of Emitter Diffusion and Screen-Printing Contact Formation on Nanostructured Silicon Surfaces. *IEEE J. Photovoltaics* **2017**, *7*, 136–143.
- (30) Cao, Y.; Zhou, Y.; Liu, F.; Zhou, Y.; Zhang, Y.; Liu, Y.; Guo, Y. Progress and Mechanism of Cu Assisted Chemical Etching of Silicon in a Low Cu²⁺ Concentration Region. *ECS J. Solid State Sci. Technol.* **2015**, *4*, P331–P336.
- (31) Wang, S.-D.; Chen, T.-W. Texturization of Diamond-Wire-Sawn Multicrystalline Silicon Wafer Using Cu, Ag, or Ag/Cu as a Metal Catalyst. *Appl. Surf. Sci.* **2018**, *444*, 530–541.
- (32) Zheng, C.; Shen, H.; Pu, T.; Jiang, Y.; Tang, Q.; Yang, W.; Chen, C.; Rui, C.; Li, Y. High-Efficient Solar Cells by the Ag/Cu-

Assisted Chemical Etching Process on Diamond-Wire-Sawn Multicrystalline Silicon. *IEEE J. Photovoltaics* **2017**, *7*, 153–156.

(33) Tsujino, K.; Matsumura, M.; Nishimoto, Y. Texturization of Multicrystalline Silicon Wafers for Solar Cells by Chemical Treatment Using Metallic Catalyst. *Sol. Energy Mater. Sol. Cells* **2006**, *90*, 100–110.

(34) Chong, T. K.; Bullock, J.; White, T. P.; Berry, M.; Weber, K. J. Nanoporous Silicon Produced by Metal-Assisted Etching: A Detailed Investigation of Optical and Contact Properties for Solar Cells. *IEEE J. Photovoltaics* **2015**, *5*, 538–544.